A&A 610, A78 (2018)
https://doi.org/10.1051/0004-6361/201730903


Astronomy & Astrophysics

# Stringent upper limit of $CH_4$ on Mars based on SOFIA/EXES observations

S. Aoki[1,2,3], M.J. Richter[4], C. DeWitt[4], A. Boogert[5,6], T. Encrenaz[7], H. Sagawa[8], H. Nakagawa[3], A. C. Vandaele[1], M. Giuranna[9], T. K. Greathouse[10], T. Fouchet[7], A. Geminale[9], G. Sindoni[9], M. McKelvey[6], M. Case[4], and Y. Kasaba[3]

[1] Planetary Aeronomy, Belgian Institute for Space Aeronomy, 3 av. Circulaire, 1180 Brussels, Belgium
e-mail: shohei.aoki@aeronomie.be
[2] Fonds National de la Recherche Scientifique, rue d'Egmont 5, 1000 Brussels, Belgium
[3] Department of Geophysics, Tohoku University, Sendai, Miyagi 980-8578, Japan
[4] Physics Department, University of California, Davis, CA 95616, USA
[5] Institute for Astronomy, University of Hawaii, Honolulu, HI 96822, USA
[6] Universities Space Research Association, Stratospheric Observatory for Infrared Astronomy, NASA Ames Research Center, MS 232-11, Moffett Field, CA 94035, USA
[7] LESIA, Observatoire de Paris, PSL Research University, CNRS, Sorbonne Universités, UPMC Univ. Paris 06, Univ. Paris Diderot, Sorbonne Paris Cité, 5 place Jules Janssen, 92195 Meudon, France
[8] Faculty of Science, Kyoto Sangyo University, Motoyama, Kamigamo, Kita-ku, Kyoto 603-8555, Japan
[9] Istituto di Astrofisica e Planetologia Spaziali, Istituto Nazionale di Astrofisica, Via del Fosso del Cavaliere 100, 00133 Roma, Italy
[10] Southwest Research Institute, Div. ♯15, San Antonio, TX 78228, USA

Received 31 March 2017 / Accepted 20 October 2017

**ABSTRACT**

Discovery of $CH_4$ in the Martian atmosphere has led to much discussion since it could be a signature of biological and/or geological activities on Mars. However, the presence of $CH_4$ and its temporal and spatial variations are still under discussion because of the large uncertainties embedded in the previous observations. We performed sensitive measurements of Martian $CH_4$ by using the Echelon-Cross-Echelle Spectrograph (EXES) onboard the Stratospheric Observatory for Infrared Astronomy (SOFIA) on 16 March 2016, which corresponds to summer ($Ls$ = 123.2°) in the northern hemisphere on Mars. The high altitude of SOFIA (~13.7 km) enables us to significantly reduce the effects of terrestrial atmosphere. Thanks to this, SOFIA/EXES improves our chances of detecting Martian $CH_4$ lines because it reduces the impact of telluric $CH_4$ on Martian $CH_4$, and allows us to use $CH_4$ lines in the 7.5 $\mu$m band which has less contamination. However, our results show no unambiguous detection of Martian $CH_4$. The Martian disk was spatially resolved into 3 × 3 areas, and the upper limits on the $CH_4$ volume mixing ratio range from 1 to 9 ppb across the Martian atmosphere, which is significantly less than detections in several other studies. These results emphasize that release of $CH_4$ on Mars is sporadic and/or localized if the process is present.

**Key words.** planets and satellites: atmospheres

## 1. Introduction

The presence of $CH_4$ in the Martian atmosphere has led to much discussion since it could be a signature of ongoing and/or past biological and/or geological activities on Mars. After preliminary detections from ground-based observations being reported in scientific meetings (Mumma et al. 2003), the first detection of $CH_4$ on Mars was published from the observations by the Planetary Fourier Spectrometer (PFS) onboard the Mars Express (MEx) spacecraft (Formisano et al. 2004). The mean abundance of $CH_4$ was found to be ~10 ppb. In the same year, detection of $CH_4$ by ground-based observations with the Canada-France-Hawaii Telescope (CFHT)/Fourier Transform Spectrometer (FTS) was also published (Krasnopolsky et al. 2004). These discoveries of $CH_4$ on Mars were remarkable because its source could be either biological activity (e.g., subsurface micro-organisms) and/or hydrothermal activity (e.g., serpentinization, Atreya et al. 2007). Identification of the source of $CH_4$ is very valuable for advancing not only planetary science but also future life explorations on Mars.

So far, the remote-sensing observations of Martian $CH_4$ has been investigated mainly by four groups, two from spacecraft-borne observations (Geminale et al. 2008, 2011; Fonti & Marzo 2010), and two from ground-based observations (Mumma et al. 2009; Krasnopolsky 2012; Villanueva et al. 2013). The spacecraft-born PFS measurements showed the variations of $CH_4$ amounts depending on season, location, and local time on Mars (Geminale et al. 2008, 2011). In particular, an enhancement of $CH_4$ (~60 ppb) over the north polar cap during the northern summer was reported, which implied the possible presence of a $CH_4$ reservoir associated with the polar cap (Geminale et al. 2011). In contrast, Fonti & Marzo (2010) analyzed the data obtained with another spacecraft-born instrument, Thermal Emission Spectrometer (TES) onboard Mars Global Surveyor (MGS), and found substantially different spatial and seasonal distributions, with peak abundance near 70 ppb over low-latitudes (Tharsis, Arabia Terra, and Elysium). Meanwhile, the other two groups investigated $CH_4$ on Mars using high-resolution, infrared spectrographs on ground-based facilities. Mumma et al. (2009) found extended plumes of

$CH_4$ (~40 ppb) during the northern summer over low-latitude regions from IRTF/CSHELL observations performed on 11–13 January 2003 ($Ls = 122°$), 19–20 March 2003 ($Ls = 155°$), and 29 May 2005 ($Ls = 220°$) – but they found no $CH_4$ on 16 January using Keck/NIRSPEC nor 26 February 2006 using IRTF/CSHELL near the vernal equinox ($Ls = 357.3°$and 17.2°). The same group reported no detection of $CH_4$ on 6 January 2006 using IRTF/CSHELL and Keck/NIRSPEC, nor with VLT/CRIRES in 2009 and Keck/NIRSPEC in 2010 (Villanueva et al. 2013). They derived an upper limit of 7 ppb from those non-detection observations, which is generally smaller than the seasonal variations reported by the spacecraft-borne measurements groups. By contrast, Krasnopolsky (2012) claimed the detection of $CH_4$ (0–20 ppb) over Valles Marines using ground-based IRTF/CSHELL observations performed on 10 February 2006, just 28 days after the Villanueva et al. (2013) observations, where no $CH_4$ had been observed over the same region (upper limit 7.8 ppb).

In short, these remote-sensing observations suggest a significant variability of $CH_4$ in space and time. The transport and/or diffusion times of days to weeks causes rapid plume dispersal, while the loss of global methane over a span from March 2003 to January 2006 requires a lifetime less than four Earth years and perhaps as short as 0.6 Earth years (Mumma et al. 2009). In contrast, the standard photochemical models showed that the lifetime of $CH_4$ in the Martian atmosphere is about 300–600 years (Lefèvre & Forget 2009), and, as a consequence, $CH_4$ should be uniformly distributed in the atmosphere. This discrepancy between the observed variability and the model prediction has led to much debate on the reliability of the previous remote-sensing observations. The reason behind such a debate is that the detected signal of $CH_4$ is very weak and the observations had a large uncertainty because of contamination of terrestrial lines and the need for a high signal-to-noise ratio. The previous ground-based observations used lines in the P-branch or R-branch of 3.3 $\mu$m band. The widths of these lines (half width at half maximum, HWHM) are about 0.006 $cm^{-1}$, which is between five and ten times narrower than the spectral resolutions of CSHELL, NIRSPEC and CRIRES. In addition, the terrestrial atmosphere hampers the observation due to telluric $CH_4$ and its isotopes (see Fig. 1); their contribution to the observed spectrum must be separated from the Martian $CH_4$ contribution to the spectrum. On the other hand, spacecraft-born observations (i.e., MGS/TES and MEx/PFS) are free from such contamination of the terrestrial atmosphere. However, their spectral resolutions are not enough for an unambiguous identification of $CH_4$. Even at the highest spectral resolution of PFS (~1.3 $cm^{-1}$) and even the fact that PFS observes the strongest lines of the Q-branch of 3.3 $\mu$m band, the absorption depth of 10 ppb of $CH_4$ yields only about one percent of the continuum emission, which is difficult to distinguished from side lobes caused by strong solar lines. The spectral resolution of the TES instrument is approximately five times worse than that of PFS. Indeed, Fonti et al. (2015) carefully revisited their previous results from the MGS/TES measurements, and concluded that they are either not able to be confirmed or refuted.

Very recently, in-situ observations of $CH_4$ on Mars were performed by the Tunable Laser Spectrometer (TLS) onboard Curiosity rover (Webster et al. 2013, 2015). The TLS detected a $CH_4$ signal which showed strong variability in magnitude (0–9 ppb). However, since TLS can measure $CH_4$ variation only on the Gale crater (which is the landing site of the rover), sensitive remote-sensing observations with a wide spatial coverage are still important in searching for the source.

The Echelon-Cross-Echelle Spectrograph (EXES) onboard the Stratospheric Observatory for Infrared Astronomy (SOFIA) is uniquely capable of performing a sensitive search for $CH_4$ from Earth. Through the entire spectral range, the strongest $CH_4$ lines are located at 3.3 $\mu$m and 7.5 $\mu$m. Figure 1 shows the terrestrial and Martian spectra around the $CH_4$ lines at 3038.498 $cm^{-1}$ (3.291 $\mu$m) and 1327.0742 $cm^{-1}$ (7.535 $\mu$m), that are simulated for the IRTF/CSHELL and SOFIA/EXES observations, respectively. As shown in Fig. 1, one of the advantages of the 7.5 $\mu$m band is less contamination of minor terrestrial lines such as $^{13}CH_4$ or $O_3$ even though the intrinsic intensities of the $CH_4$ lines at 3.3 $\mu$m and 7.5 $\mu$m are comparable. However, the Martian $CH_4$ line in this 7.5 $\mu$m band cannot be accessed from the ground-based observations because the Doppler shift (due to Martian motion with respect to Earth) of the line frequency is about half of that of 3.3 $\mu$m and thus the Martian lines are buried in the strong absorption of terrestrial $CH_4$. Encrenaz et al. (2005) attempted to search for $CH_4$ on Mars using IRTF/TEXES in the mid-infrared spectral range, however, they could not use the strongest lines because of the deep terrestrial $CH_4$ absorption. This imposed a limitation on their data (derived upper limits were 20 ppb in the morning side and 70 ppb in the evening side). The situation changes drastically for SOFIA thanks to the higher altitude (~13.7 km). With SOFIA, Martian $CH_4$ lines at the 7.5 $\mu$m band can be measured in the wing of the terrestrial lines, which makes this air-borne facility unique compared to any ground-based facilities including those located at the summit (~4 km in the altitude) of Mauna Kea. In order to detect the narrow Martian $CH_4$ lines located at the wings of the deep terrestrial line, high spectral resolution is essential. The EXES instrument realizes high spectral resolution of ~90 000, and it largely improves the chances to detect $CH_4$ lines although the Martian lines are not fully resolved. One of the disadvantages at 7.5 $\mu$m is that the signals depend on the thermal contrast between the surface and atmosphere on Mars because the $CH_4$ line is formed in the thermal emission regime. Nevertheless, thanks to SOFIA's high altitue, SOFIA/EXES can provide comparable or better (by a few) absorption depths of Martian $CH_4$ than those from previous ground-based observations. Moreover, EXES has the additional advantage that we can measure multiple $CH_4$ lines simultaneously, which allows us to improve the accuracy of the $CH_4$ retrieval.

In this study, we describe the results of our sensitive search for $CH_4$ on Mars using SOFIA/EXES. The details of the SOFIA/EXES observations and data analysis are described in Sects. 2 and 3, respectively. The observational results are discussed in Sect. 4.

## 2. Observations

SOFIA is an airborne observatory consisting of a specially modified Boeing 747 SP with a 2.7 m diameter telescope flying at altitudes as high as 13.7 km (Young et al. 2012). EXES is an infrared grating spectrograph onboard the SOFIA telescope. It is derived from the Texas Echelon Cross Echelle Spectrograph (TEXES) instrument in operation at NASA IRTF and Gemini-North (Lacy et al. 2002). EXES operates in the spectral ranges between 4.5 and 28.3 $\mu$m (2220–350 $cm^{-1}$), with high spectral resolution mode ($R$ = 50 000–100 000), medium resolution mode ($R$ = 5000–20 000), and low resolution mode ($R$ = 1000–3000). The instrument is equipped with a 1024 × 1024 Si:As detector array. The high-resolution mode is provided by a steeply blazed aluminum reflection grating used as an echelon,

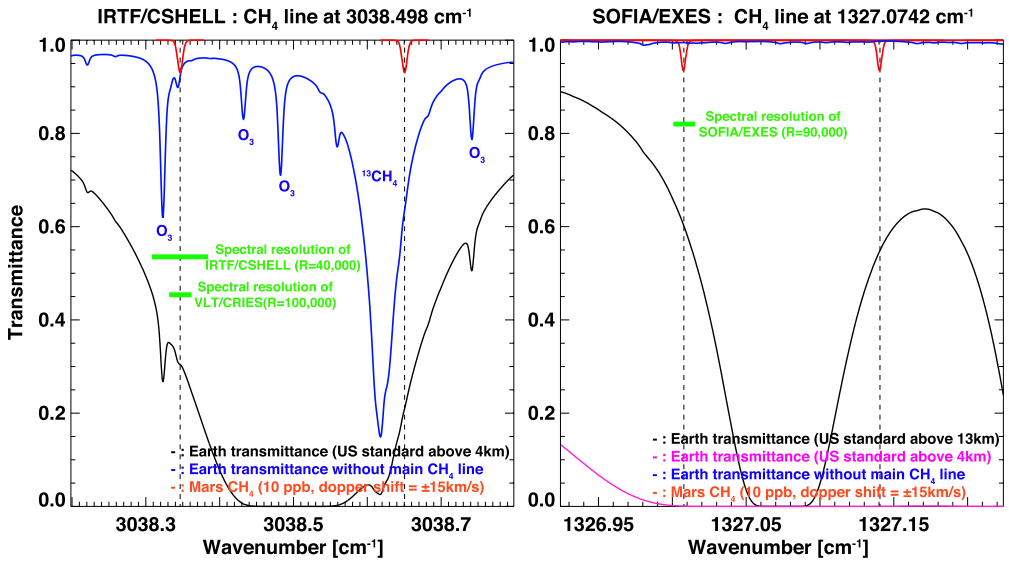


**Fig. 1.** Synthetic spectra around the $CH_4$ line at 3038.498 $cm^{-1}$ (*left*) and at 1327.0742 $cm^{-1}$ (*right*). The former spectral region was used for the previous observations performed by IRTF/CSHELL, Keck/NIRSPEC, and VLT/CRIRES (Mumma et al. 2009; Villanueva et al. 2013), and the latter spectrum was used for the SOFIA/EXES observations. The black and blue curves in the *left-hand figure* represent the transmittance with/without the main $CH_4$ line due to terrestrial atmosphere calculated from US standard atmosphere above 4 km (which is the altitude of Mauna Kea Observatory) with airmass = 1.4 (which is the minimum airmass during the observation on 20 March 2003 by Mumma et al. 2009.). The black and blue curves in the *right-hand figure* are the transmittances calculated from US standard atmosphere above 14 km (which is the altitude of SOFIA) with airmass = 2.0 (which is the maximum airmass during our observation on 16 March 2016). The purple curve shown in the *right figure* is the same as black one but from US standard atmosphere above 4 km. The red curves shown in both figures are absorption depth due to 10 ppb of Martian $CH_4$ with the Doppler shift between Mars and Earth being ±15 km $s^{-1}$. The green bars shown in the *left and right figures* represent the spectral resolutions of IRTF/CSHELL and VLT/CRIRES, and that of SOFIA/EXES, respectively.

**Table 1.** Overview of the SOFIA/EXES observations.

| Date and time (UT) | *Ls* (°) | MY | Doppler shift (km/s) | Diameter of Mars (″) | Aircraft altitude (km) | Silt positions and integration times (min) | Sub-Earth longitude (°W) | Spectral range ($cm^{-1}$) | Telescope elevation (°) |
|---|---|---|---|---|---|---|---|---|---|
| 16/March/2016 9:59–10:32 | 123.2 | 33 | −16.2 | 10.0 | 13.7 | Mars Center ♯1: 9<br>Mars Center ♯2: 6<br>Mars Left 2.5″: 9<br>Mars Right 2.5″: 9 | 213–220 | 1326.57–1338.66 | 30.2–32.3 |

associated with an echelle grating to cross-disperse the spectrum (Richter et al. 2010).

Our observations made using SOFIA/EXES were performed on 16 March 2016 (see Table 1). The observations were performed when SOFIA was flying at 13.7 km. The observed season on Mars corresponds to summer (*Ls* = 123.2°) in the northern hemisphere. The diameter of Mars was 10.0 arcsec. The Doppler shift between Mars and Earth was −16.2 km $s^{-1}$. During the observation, the longitude of the sub-Earth and sub-solar points varied from 213°W to 220°W, and from 247°W to 253°W, respectively. The latitude of these points was 7.7°N (sub-Earth) and 21.1°N (sub-solar). For our search of $CH_4$ on Mars, we selected the 1326–1338 $cm^{-1}$ (7.47–7.54 $\mu$m) interval considering the availability of multiple strong $CH_4$ lines, and used the high-spectral resolution mode to improve the possibility of detecting the narrow Martian lines. The narrowest slit-width (1.44 arcsec) was used to maximize the spectral resolving power that provided an instrumental resolving power of ∼90 000. The slit length is 10.69″ (0.18 arcsec $pix^{-1}$), which is comparable to the diameter of Mars (10.0″). Figure 2 illustrates the configuration of the slit positions. The slit was oriented at a position angle of 260°. As shown in Fig. 2, we observed the planet at three separate slit positions: which we called center, right, and left of the Martian disk. For the right and left positions, the center of the slit was offset by 2.5″ perpendicular to the slit angle. At each slit position, we observed Mars for several minutes to reach the signal to noise ratio of more than ∼200 with respect to the continuum emission. During the observations, we nodded the telescope 42 arcsec to observe blank sky. Subtraction of the A (Mars) and B (blank sky) beams removes background emission and telluric night sky emission, although an airmass dependent contribution to the night sky emission would remain as the airmass steadily changes, assuming the atmosphere is otherwise constant. With the Doppler shift moving Martian $CH_4$ away from telluric $CH_4$, we believe any such residual does not impact our analysis as described below. In addition, we observed alpha Lyr as a telluric calibration star.

An example of the spectrum measured with EXES is shown in Fig. 3. We recorded 17 different spectral orders, covering 1326.57–1338.66 $cm^{-1}$. The spectral coverage of EXES allows us to observe not only $CH_4$ but also $H_2O$, HDO, and $CO_2$ lines. The spatial resolution of SOFIA at the time of the observations was 3 arcsec, which is several times larger than those by the previous ground-based observation because of poor image

**Table 2.** Parameters of $CH_4$ lines used in this study.

| Wavenumber ($cm^{-1}$) | Intensity [cm] (for 296 K) | Lower-state energy ($cm^{-1}$) | Upper-state "global" quanta | Lower-state "global" quanta | Upper-state "local" quanta | Lower-state "local" quanta |
|---|---|---|---|---|---|---|
| 1327.074219 | 9.631E-20 | 62.8781 | 0 0 0 1 1F2 | 0 0 0 0 1A1 | 4A1 1 | 3A2 1 |
| 1327.409783 | 5.781E-20 | 62.8757 | 0 0 0 1 1F2 | 0 0 0 0 1A1 | 4F2 1 | 3F1 1 |
| 1332.546743 | 5.732E-20 | 104.7746 | 0 0 0 1 1F2 | 0 0 0 0 1A1 | 5F2 1 | 4F1 1 |

**Notes.** The values are taken from the HITRAN 2012 spectroscopic database (Rothman et al. 2013). Upper and lower state "global" quanta are described using the HITRAN notation (Rothman et al. 2005): *v1 v2 v3 v4 n C*, where $v_j$ is the quantum number associated with the normal mode of vibration *j*, *n* is a multiplicity index and *C* (=*A1, A2, F1, F2*, and *E*) is the symmetry. Upper and lower state "local" quanta are described using the Brown et al. notation (Brown et al. 2003): *J C* $\alpha$, where *J* is the quantum number associated with the total angular momentum excluding nuclear spin, *C* (=*A1, A2, F1, F2,* and *E*) is the symmetry and $\alpha$ is a counting integer for levels of the same *J* and *C*; the values are incremented in order of increasing energy.

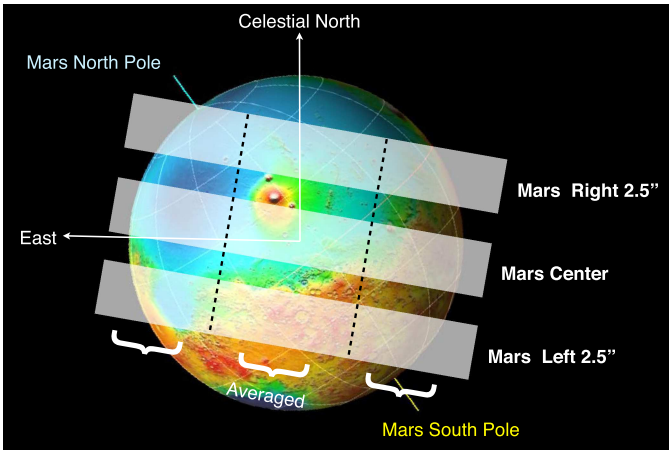


**Fig. 2.** Geometry of the Mars observations taken by SOFIA/EXES. The instrument slit was oriented at a position angle of 260°. The slit is indicated as *white boxes*, and were put at the three separate slit positions: "Mars Center", "Mars Right 2.5", and "Mars Left 2.5". For the center position, the slit was placed over the sub-Earth point. For the right and left positions, we offset the center of the slit to 2.5″ perpendicular to the slit angle. In this analysis, the measured spectra were binned over 15 pixels (~2.7″) along the slit in order to increase the signal to noise ratio. As a consequence, three averaged spectra were obtained for each slit position.

quality of the SOFIA observatory. This corresponds to a latitudinal and longitudinal resolution of about ±27° (~2000 km in the horizontal scale) at the sub-Earth point.

## 3. Data analysis

### 3.1. Extraction of the Martian features

We searched for $CH_4$ on Mars using multiple lines. As shown in Fig. 3, there are 11 strong $CH_4$ absorption lines in the selected spectral range. We confined our analysis to three lines that have no contamination from other lines (i.e., terrestrial $CH_4$ and $H_2O$, and Martian $CO_2$ and $H_2O$ lines) and stronger intensities than the other $CH_4$ lines. Table 2 describes the $CH_4$ lines used for this analysis. The line parameters were obtained from the HITRAN 2012 database (Rothman et al. 2013).

In order to increase the signal to noise ratio, the measured spectra were binned over 15 pixels (~2.7″) along the slit which binning size is determined from the spatial resolution of the telescope. As a consequence, three averaged spectra were obtained for each slit position (see Fig. 2). The Martian $CH_4$ lines should appear on the wings of the deep terrestrial lines. Figure 4a shows an example of an averaged EXES spectra around the $CH_4$ line at 1327.074219 $cm^{-1}$. As shown in Fig. 4a, the terrestrial and Martian $CH_4$ lines were clearly separated. Then, the absorption feature of Martian $CH_4$ lines were examined by fitting a local continuum level around the $CH_4$ lines. This local continuum was determined by fitting the averaged spectra with a cubic polynomial for the spectral interval of 25 points centered at the Martian $CH_4$ lines. The fitting did not include 17 center points where Martian $CH_4$ is expected. Figure 4b shows an example of the local continuum determined by the cubic polynomial fit. The Martian $CH_4$ lines were extracted by obtaining the deviation of the observed spectrum from the local continuum, and then they were compared with synthetic spectra calculated by radiative transfer model.

### 3.2. Modeling of synthetic spectra

We performed radiative transfer calculations to evaluate (the upper limit on) $CH_4$ abundances in the extracted Martian features. We used a fast and accurate radiative transfer model that includes multiple scattering effects (Ignatiev et al. 2005). The calculation was performed in the spectral ranges between 1325 and 1340 $cm^{-1}$. Dust, water ice clouds, $CO_2$ gas, and $CH_4$ gas absorption were taken into account in the calculation. The vertical domain in the modeled Mars atmosphere was represented by 80 layers which covers altitudes from the surface to 80 km with uniform thickness of 1 km. The absorption coefficients of $CO_2$ and $CH_4$ gases were calculated based on the line-by-line method with a spectral sampling of 0.00025 $cm^{-1}$ (about 1/60 of the spectral resolution of the measurements) using the HITRAN 2012 database (Rothman et al. 2013). For the line shape function, a Voight function was adopted (Kuntz 1997; Ruyten 2004). The single scattering optical properties of dust and water ice clouds were calculated with the Mie theory (Wiscombe 1980) and then integrated with the modified gamma distribution (Kleinböhl et al. 2009). The refractive indices of dust and water ice were from the works by Wolff & Clancy (2003) and Warren (1984), respectively.

Geometry and orbital parameters during the observations such as emission angles, latitude, and longitude of Mars were obtained from the NASA-JPL ephemeris generator[1]. Based on that, we computed the synthetic spectra over the Martian disk with an interval of 0.25 arcsec. Surface temperatures and vertical profiles of temperature, pressure, dust, water ice clouds, and $CO_2$ volume mixing ratio were extracted from the Mars Climate database (MCD) Version 5.2 for the each spatial point over the Martian disk (Millour et al. 2015). In order to take into account

[1] http://ssd.jpl.nasa.gov/horizons.cgi

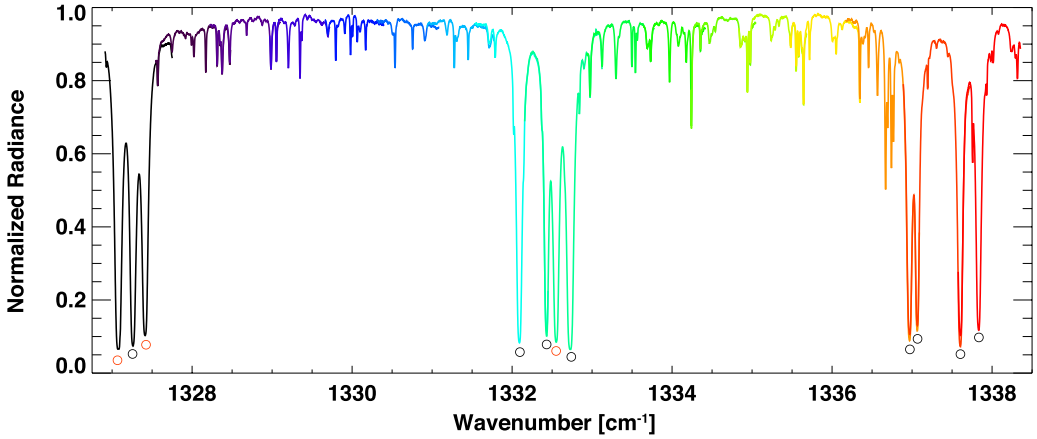


**Fig. 3.** Example of a Mars spectrum obtained by SOFIA/EXES, spatially integrated over the entire slit. Differences in colors show the 17 spectral orders. The spectrum was observed on 16 March 2016 with nine minutes integration. Circular symbols represent the strong terrestrial $CH_4$ lines. The red ones are the $CH_4$ lines that are used in this analysis. The other lines visible in this spectrum are $H_2O$, HDO, $CO_2$ (628), and $CO_2$ (638).

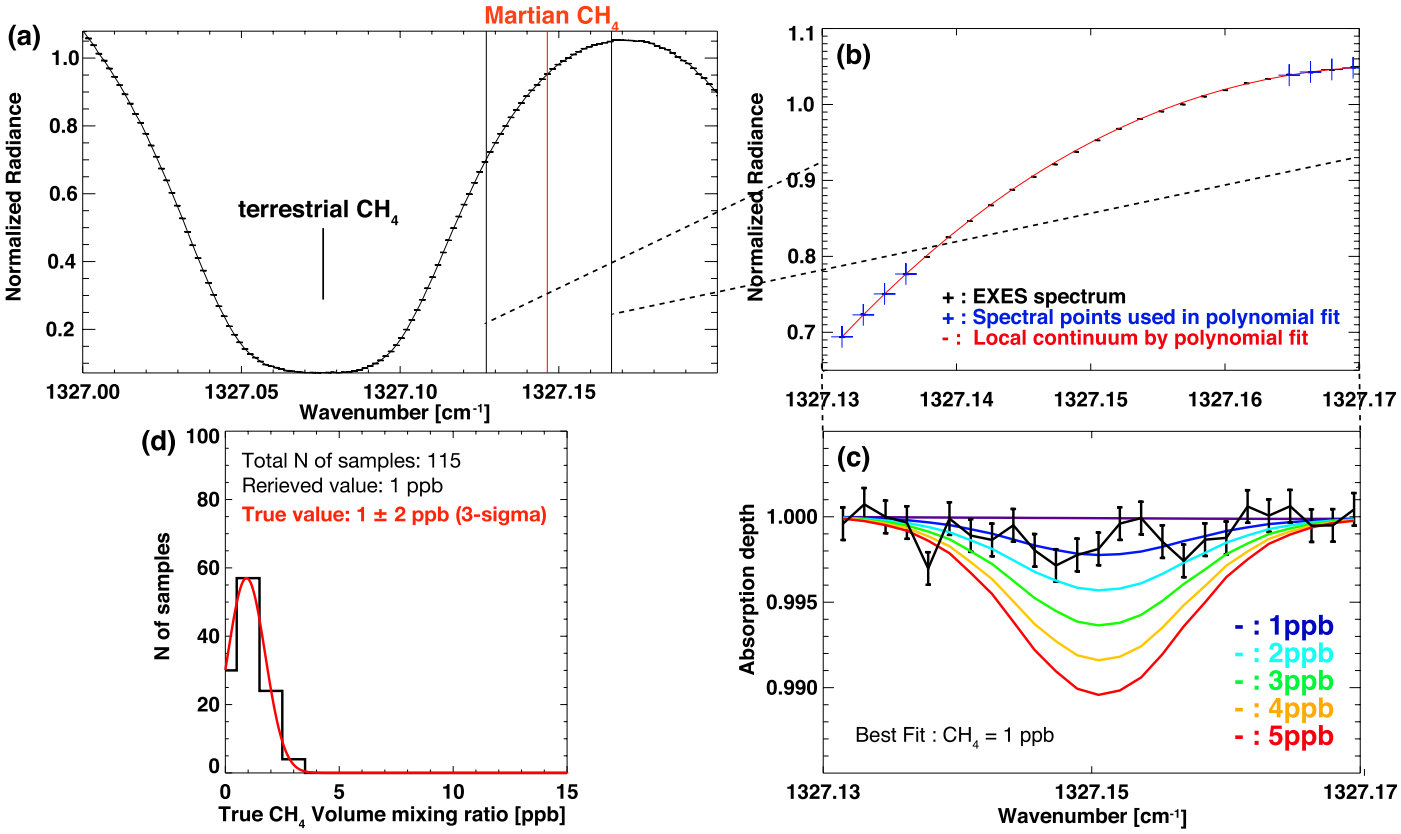


**Fig. 4.** Example of data analysis. *Panel a*: black curve shows the averaged EXES spectrum (over one-third of the entire slit) in the spectral range between 1327.0 and 1327.2 $cm^{-1}$. The slit position is "Mars Center ♯1", and the mean Latitude, Longitude, and Local time of the averaged spectrum are 40°N, 247°W, and 12h, respectively. The strong absorption due the terrestrial $CH_4$ is visible at 1327.074219 $cm^{-1}$. The red vertical bar shows the expected spectral position of the Martian $CH_4$ line shifted due to Doppler velocity between Earth and Mars. The black bars represent the spectral range which was used for retrieval of $CH_4$ mixing ratio on Mars. *Panel b*: black points are the same EXES spectrum as shown in *panel a* but focused around the expected Martian $CH_4$ lines. The red curve shows the local continuum established by the cubic polynomial fit. The blue points represent the spectral points used to perform the cubic polynomial fit. *Panel c*: black curve shows the absorption depth spectrum due to Mars atmosphere that is the EXES spectrum divided by the local continuum. The color curves are the synthetic absorption depth with various mixing ratio of the Martian $CH_4$ (blue: 1 ppb, light blue: 2 ppb, green: 3 ppb, orange: 4 ppb, red: 5 ppb) that is the synthetic spectrum with the Martian $CH_4$ divided by the one without the Martian $CH_4$. The one with 1 ppb of $CH_4$ mixing ratio (the blue one) provides the minimum cost function (i.e., the best-fit synthetic spectrum). *Panel d*: true $CH_4$ mixing ratio when the retrieved $CH_4$ mixing ratio is 1 ppb. The histogram is obtained from the retrieval test using simulated EXES spectra (see Sect. 3.4). The uncertainty of this retrieval is estimated to be 2 ppb ($3\sigma$) from the histogram.

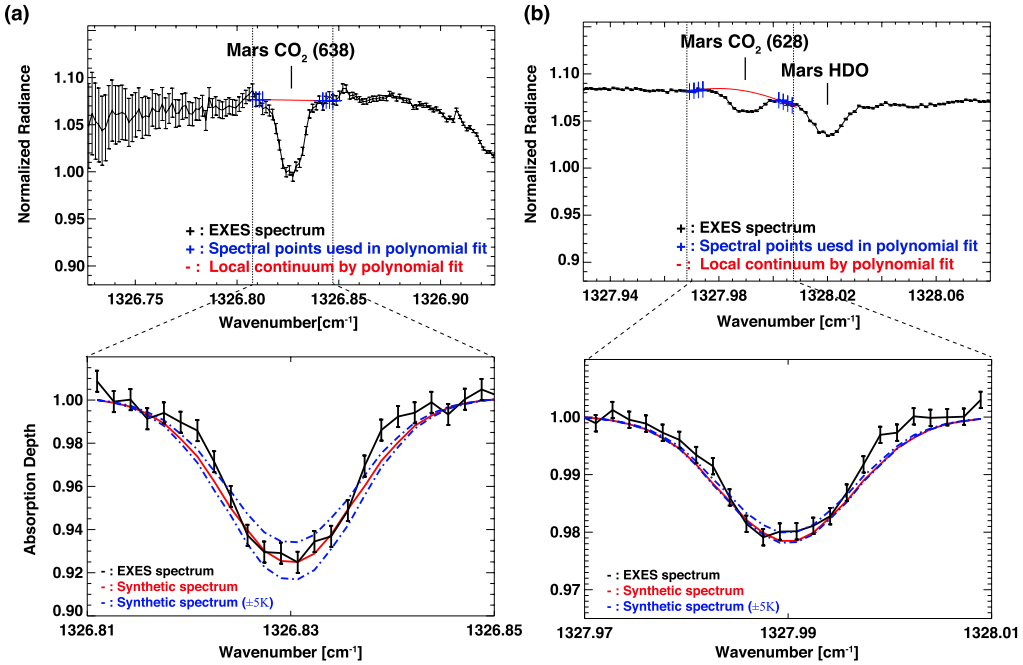


**Fig. 5.** Examples of extraction of the Martian $CO_2$ lines and their comparison with the synthetic spectra calculated by our radiative transfer codes. Those of $CO_2$ (638) line at 1326.75438 $cm^{-1}$ and $CO_2$ (628) line at 1327.917522 $cm^{-1}$ are shown in *panels a* and *b*, respectively. The positions of these lines are shifted due to the Doppler velocity between Mars and Earth. The black curves shown in the *upper panels* are the averaged EXES spectrum. The slit position is "Mars Center ♯1", and the mean Latitude, Longitude, and Local time of the averaged spectrum are 17°S, 181°W, and 16 h, respectively. In the *upper panel of panel b*, an absorption band due Martian HDO is also visible. We note that error values in the left wing of the Martian $CO_2$ (638) line are relatively high because they are close to the edge of the slit. The red curves and blue points in the *upper panels* show the local continuums established by the cubic polynomial fit and the spectral points used to perform the cubic polynomial fit, respectively. In the *lower panels*, the black curves represent the transmittance spectra due to Mars atmosphere that are the EXES spectrum divided by the local continuum. The red curves are synthetic spectra calculated with the vertical temperature profiles extracted from MCD, and the blue curves show the ones with the temperature profiles shifted by ±5 K. The extracted spectral features of the Martian $CO_2$ lines show a good agreement with the synthetic spectra even though there is a small disparity appeared in the wings.

the spatial resolution of the observations, the calculated synthetic spectra were synthesized with a two-dimensional Gaussian function with a full width at half maximum (FWHM) of 3 arcsec. The synthesized spectra were averaged over the expected slit position to be compared with the measured spectra. The averaged synthetic spectra were finally convolved in a wavelength domain with another Gaussian function that corresponds to the spectral resolution of EXES ($R$ = 90 000; ~9 pixels).

### 3.3. Validation of the data reduction methodology

To check the validity of the extraction method and calculation of synthetic spectra, the algorithm was applied to Martian $CO_2$ lines as well. For this purpose, a weak $CO_2$ isotope (638) line at 1326.75438 $cm^{-1}$ and $CO_2$ isotope (628) line at 1327.917522 $cm^{-1}$ were selected. The line intensity of the $CO_2$ (638) line is $9.662 \times 10^{-27}$ cm at 296 K with an uncertainty range between 2% and 5%, and that of the $CO_2$ (628) line is $1.883 \times 10^{-26}$ cm with an uncertainty range being more than 20% (Rothman et al. 2013). Figure 5 shows examples of the extraction of these $CO_2$ lines by using the local continuum determined by the cubic polynomial fit, and their comparison with the synthetic spectra calculated by our radiative transfer model. The Martian $CO_2$ (638) line yields about 10% of absorption depth respect to the continuum emission, while the $CO_2$ (628) line does a few percent of absorption because the Lower-state energy $E''$ of the $CO_2$ (628) line ($E''$ = 1052.7719 $cm^{-1}$) is larger than that of $CO_2$ (638) line ($E''$ = 170.0769 $cm^{-1}$). The extracted spectral features of the Martian $CO_2$ lines show a good agreement with the synthetic spectra (we note that the volume mixing ratio of $CO_2$ considered in the synthetic spectra is the one extracted from MCD, and the isotopic ratio of $CO_2$ is the terrestrial one included in HITRAN 2013). We note the small disparity remaining between measured and synthetic spectra at the wings of the $CO_2$ lines. It might be due to the fact that a Gaussian function is not appropriate in the wings of the instrumental line shape of EXES, however, its effect on analyzing weak $CH_4$ signals is negligible compared with the amplitude of the measurement noise.

### 3.4. Retrieval of $CH_4$ mixing ratio

The synthetic spectra were calculated for $CH_4$ volume mixing ratios ranging from 0 ppb to 50 ppb with intervals of 1 ppb, and the best-fit $CH_4$ mixing ratio was determined by minimizing the cost function $C$. The cost function was defined as

$$C = \Sigma(Y_{obs} - Y_{model})^2, \quad (1)$$

where $Y_{model(x)}$ is the absorption depth of synthetic spectra which is the synthetic spectra with $CH_4$ divided by the one without $CH_4$, and $Y_{obs}$ is the absorption depth of the EXES spectra which is the original SOFIA spectra divided by continuum simulated via Cubic polynomial fitting (as described in Sect. 3.1). The cost functions were calculated using the spectral interval of 25 points centered at the Martian $CH_4$ lines. The retrievals were performed independently for each line of the selected three $CH_4$ lines. Figure 4c shows an example of the comparison between the absorption depth of the EXES spectra and synthetic ones. There are three sources of error in the retrieved $CH_4$ volume mixing

ratio: (1) instrumental noise on the measured spectra, (2) method of analysis itself (such as imperfect subtraction of the continuum baseline), and (3) uncertainty in the vertical temperature profile used in the radiative transfer calculation. The error due to the former two reasons was estimated via statistics using simulated EXES spectra and the following steps:

– Simulated EXES spectra in the relevant spectral region were calculated using the spectral resolution and sampling of the actual measurements considering the US standard Earth atmosphere above 14 km with the airmass set to match the actual observation condition. Mars atmospheric absorption due to $CO_2$ gas is also included in this simulated spectra. Instrumental noise was input to the simulated EXES spectra. The instrumental noise were defined by

$$Noise = \sqrt{\frac{C}{N}} \times \xi, \quad (2)$$

where $N$ is the number of spectral points (i.e., 25) and $\xi$ is a random number following a Gaussian distribution ($\sigma = 1$). The first value in the equation represents the standard deviation between the best-fit model and the measured EXES spectra. To initialize the random number, a total of 100 different "seed" values were used (i.e., we have different 100 noise patterns in total).

– Martian $CH_4$ absorptions were additionally included to the simulated EXES spectra. $CH_4$ volume mixing ratios from 0 to 30 ppb with intervals of 1 ppb were considered (i.e., 3100 simulated EXES spectra were obtained in the end).

– The $CH_4$ retrieval algorithm, which we used for the data analysis of the real measurement data, was applied to these simulated EXES spectra in a similar way. Such retrieval tests provide an estimate on the accuracy of the retrieved $CH_4$ mixing ratios. Figure 4d shows an example of our retrieval test.

To evaluate the third source of error, we first estimated the uncertainty in the vertical temperature profile by comparing between measured and modeled absorption depth at the $CO_2$ lines (see detail in the Sect. 3.3). From the comparison, we concluded that the uncertainty in the temperature profile is within 5 K (see Fig. 5 as an example). Then, the retrieval of the $CH_4$ volume mixing ratio was performed with the temperature profile uniformly shifted by ±5 K, the error was defined as the differences between those results and original ones. Finally, the uncertainties in the retrieved $CH_4$ volume mixing ratio for each lines ($\sigma_{line}$) is given by

$$\sigma_{line} = \sqrt{\sigma_n^2 + \sigma_m^2}, \quad (3)$$

where $\sigma_n$ is the error due to method of analysis itself and instrumental noise, and $\sigma_m$ represents the error due to the uncertainty in the vertical temperature profile used in the radiative transfer calculation. We note that the error due to the instrumental noise is the dominant contribution. After the uncertainties were evaluated for the results of each $CH_4$ line, the $CH_4$ mixing ratios and their $3\sigma$ confidences were calculated by the weighted averages using the ones retrieved from three $CH_4$ lines independently (see Aoki et al. 2015, Sect. 3).

## 4. Results and discussion

Table 3 summarizes the $CH_4$ volume mixing ratios independently retrieved from the selected $CH_4$ lines, their weighted averages, and the corresponding locations (latitude and longitude) and local times. The results from three lines were all consistent within $3\sigma$. As shown in Table 3, there are no definitive detections of $CH_4$. The upper limits range from 1 to 9 ppb which are more stringent than those by the previous remote-sensing observations.

Mumma et al. (2009) detected $CH_4$ in the northern summer in MY26. Figure 6 shows the comparison between spatial distribution of $CH_4$ reported by Mumma et al. (2009) and the FOV of our SOFIA/EXES observations. Mumma et al. (2009) had reported the presence of extended plumes (25–40 ppb) at late northern summer ($Ls = 155°$) over Terra Sabae (20°S–30°N, 300–330°W), and Nili Fossae and Syrtis Major (10°S–30°N, 270–300°W). The SOFIA/EXES observation did not properly cover Terra Sabae but a part of Nili Fossae and Syrtis Major. As roughly 30 percent of the FOV of our analyzed SOFIA/EXES measurement corresponds to the signal from Nili Fossae and Syrtis Major, our measurements are capable of detecting such a $CH_4$ plume even though the $CH_4$ mixing ratio to be detected is attenuated. However, the results show that $CH_4$ mixing ratio of 1 ± 2 ppb for the location covering Nili Fossae and Syrtis Major. The red spectrum shown at the lower left corner of Fig. 6 represents the simulated EXES spectrum that would be observed if $CH_4$ abundances were as large as those reported by Mumma et al. (2009). The spectrum is simulated with the spatially inhomogeneous, localized $CH_4$ distribution based on the results by Mumma et al. (2009), that is, 30 ppb at 10°S–30°N, 270–300°W, and 15 ppb at 15°S–60°N, 260–300°W (the observation geometry of "Mars Left" slit-position is also assumed). It shows a clear absorption feature by an absorption depth of 2.5 percent, which is more significant than the noise level of our actual observation (the black spectrum shown at the lower left corner of Fig. 6). Mumma et al. (2009) had also reported moderate amount of $CH_4$ (0–25 ppb) from their earlier measurements (at $Ls = 121$–$122°$ in MY 26), farther to the East where we did not detect $CH_4$ by SOFIA/EXES performed at the same season ($Ls = 123°$ in MY 33). Non-detection of $CH_4$ by SOFIA/EXES indicates that the release of $CH_4$ is very unlikely an annual event.

Fries et al. (2016) recently proposed a candidate of the $CH_4$ enhancement. Their hypothesis is that carbonaceous material is deposited into the Martian atmosphere in meteor showers and then ambient UV generates $CH_4$ from that. Indeed, the $CH_4$ plume reported by Mumma et al. (2009) was measured only a couple of days after a Mars encounter with the orbit of comet C/2007 H2 Skiff. However, Roos-Serote et al. (2016) argued that there is no correlation between high atmospheric $CH_4$ abundance and the occurrence of meteor showers after considering a full set of $CH_4$ observations including new Curiosity/TLS observations and all the predicted meteor shower events. The comet Skiff encountered Mars again on 8 March 2016, which is just eight days before we performed our observations with SOFIA/EXES. The non-detections of such $CH_4$ plumes by SOFIA/EXES support the argument that the meteor shower does not likely produce high $CH_4$ abundances in the Mars atmosphere.

The SOFIA/EXES observation also covers Gale Crater (Latitude = 4.5°S, Longitude = 137°E) where Curiosity/TLS has been measuring $CH_4$ abundances. TLS revealed that background level of $CH_4$ mixing ratio over Gale Crater is 0.69 ± 0.25 ppb, and detected higher amount of $CH_4$ mixing ratio (5–9 ppb) at $Ls = 336.5°$ in MY 31 and $Ls = 55°$–$82°$ in MY 32 (Webster et al. 2015). However, in MY 33, TLS does not detect such high amounts of $CH_4$ until $Ls = 94.2°$ (Roos-Serote et al. 2016). Our results show that the $CH_4$ mixing ratio covering Gale Crater is 1 ± 1 ppb, 0 ± 3 ppb, and 0 ± 1 ppb. The upper limits are

**Table 3.** $CH_4$ mixing ratio on Mars retrieved from the SOFIA/EXES observation.

| Slit position | Lat (°) | Lon[1](°) | LT[2] | $CH_4$ volume mixing ratio ($3\sigma$) | | | |
|---|---|---|---|---|---|---|---|
| | | | | 1327.0742 $cm^{-1}$ | 1327.4098 $cm^{-1}$ | 1332.5467 $cm^{-1}$ | Weighted average |
| Mars Center ♯1 | −17 | 181 | 16 | 4 ± 8 ppb | 1 ± 4 ppb | 0 ± 18 ppb | 2 ± 3 ppb |
| Mars Center ♯1 | 13 | 211 | 14 | 0 ± 2 ppb | 1 ± 2 ppb | 4 ± 6 ppb | 1 ± 1 ppb |
| Mars Center ♯1 | 40 | 247 | 12 | 1 ± 3 ppb | 1 ± 5 ppb | 0 ± 5 ppb | 1 ± 2 ppb |
| Mars Left | −42 | 205 | 15 | 2 ± 8 ppb | 0 ± 6 ppb | 0 ± 14 ppb | 1 ± 5 ppb |
| Mars Left | −8 | 237 | 13 | 0 ± 6 ppb | 0 ± 3 ppb | 2 ± 12 ppb | 0 ± 3 ppb |
| Mars Left | 13 | 270 | 11 | 2 ± 4 ppb | 0 ± 2 ppb | 3 ± 9 ppb | 1 ± 2 ppb |
| Mars Right | 0 | 168 | 18 | 10 ± 16 ppb | 1 ± 7 ppb | 0 ± 25 ppb | 3 ± 6 ppb |
| Mars Right | 30 | 189 | 16 | 0 ± 2 ppb | 1 ± 6 ppb | 2 ± 7 ppb | 0 ± 2 ppb |
| Mars Right | 66 | 218 | 14 | 0 ± 2 ppb | 0 ± 3 ppb | 1 ± 3 ppb | 0 ± 1 ppb |
| Mars Center ♯2 | −17 | 188 | 16 | 3 ± 7 ppb | 0 ± 7 ppb | 0 ± 11 ppb | 1 ± 4 ppb |
| Mars Center ♯2 | 13 | 217 | 14 | 0 ± 3 ppb | 0 ± 2 ppb | 2 ± 5 ppb | 0 ± 1 ppb |
| Mars Center ♯2 | 40 | 253 | 12 | 0 ± 2 ppb | 3 ± 6 ppb | 0 ± 4 ppb | 0 ± 2 ppb |

**Notes.** We note that EXES spectra were spatially binned over ~2.7 arcsec, which corresponds latitudinal/East-longitudinal resolution of about ±27° at the sub-Earth point. (1) West longitude; (2) Local solar time on Mars, with the LT units being 1/24th of a sol; 15 degrees of longitude.

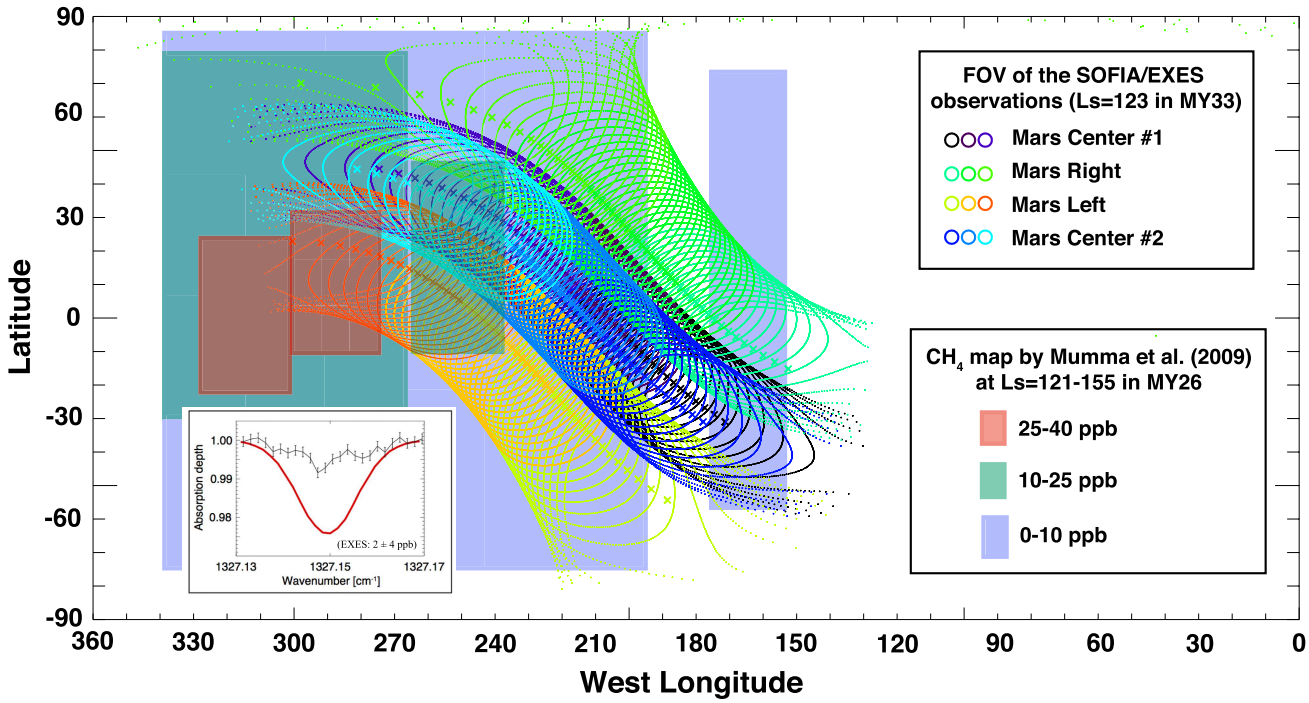


**Fig. 6.** Comparison between the spatial coverage of the SOFIA/EXES observations and spatial distribution of $CH_4$ detections reported by Mumma et al. (2009). The colored cross is the location where each pixel of the EXES detector was positioned during observation, and the distorted circles represent the field of views (FOVs), which size is 3 arcsec, for each pixel. Each color represents a set of 15 pixels which we averaged in our analysis (see Fig. 2). The filled rectangles shows the regions where Mumma et al. (2009) reported detections of $CH_4$ (red: 25–40 ppb, green: 10–25 ppb, blue: 0–10 ppb) at the northern summer ($Ls = 121–155°$) in MY26. See the main text for the *small panel embedded* at the lower left corner.

larger than the TLS-reported background level but less than the high value. The SOFIA/EXES observation was carried out at $Ls = 123.2°$ in MY 33, which is out of the seasonal range of high $CH_4$ abundance observed by TLS. One possible explanation for this non-detection of $CH_4$ by SOFIA/EXES could be due to strong temporal variation.

SOFIA/EXES is probably the most accurate remote-sensing facility for detecting $CH_4$ from Earth. However, our result did not show unambiguous detection of $CH_4$. Non-detection of $CH_4$ could be due to its strong temporal variation, similar to that measured by Curiosity/TLS over Gale crater, or to localized spatial distribution. Our results emphasize that release of $CH_4$ on Mars is sporadic and/or localized if the process is present.

*Acknowledgements.* This work has been supported by the FNRS "CRAMIC" project under grant agreement no. T.0171.16 and is based on observations made with the NASA/DLR Stratospheric Observatory for Infrared Astronomy (SOFIA). SOFIA is jointly operated by the Universities Space Research Association, Inc. (USRA), under NASA contract NAS2-97001, and the Deutsches SOFIA Institute (DSI) under DLR contract 50 OK 0901 to the University of Stuttgart. MJR, CD, and MC of the EXES team are supported by NASA award NNX13AI85A. YK and NH are supported by a Grant-in-Aid for Scientific Research (15H05209; 16K05566) from the Japanese Society for the Promotion

of Science (JSPS). HN was supported by the Astrobiology Center Program of National Institutes of Natural Sciences (NINS) (Grant Number AB281003).

## References

Aoki, S., Nakagawa, H., Sagawa, H., et al. 2015, Icarus, 260, 7
Atreya, S. K., Mahaffy, P. R., & Wong, A.-S. 2007, Planet. Space Sci., 55, 358
Brown, L., Benner, D. C., Champion, J., et al. 2003, J. Quant. Spectrosc. Radiat. Transf., 82, 219
Encrenaz, T., Bézard, B., Owen, T., et al. 2005, Icarus, 179, 43
Fonti, S., & Marzo, G. A. 2010, A&A, 512, A51
Fonti, S., Mancarella, F., Liuzzi, G., et al. 2015, A&A, 581, A136
Formisano, V., Atreya, S., Encrenaz, T., Ignatiev, N., & Giuranna, M. 2004, Science, 306, 1758
Fries, M., Christou, A., Archer, D., et al. 2016, Geochem. Perspect. Lett., 2, 10
Geminale, A., Formisano, V., & Giuranna, M. 2008, Planet. Space Sci., 56, 1194
Geminale, A., Formisano, V., & Sindoni, G. 2011, Planet. Space Sci., 59, 137
Ignatiev, N. I., Grassi, D., & Zasova, L. V. 2005, Planet. Space Sci., 53, 1035
Kleinböhl, A., Schofield, J. T., Kass, D. M., et al. 2009, J. Geophys. Res. (Planets), 114, E10006
Krasnopolsky, V. A. 2012, Icarus, 217, 144
Krasnopolsky, V. A., Maillard, J. P., & Owen, T. C. 2004, Icarus, 172, 537
Kuntz, M. 1997, J. Quant. Spec. Radiat. Transf., 57, 819
endrefcommentnewpage
Lacy, J. H., Richter, M. J., Greathouse, T. K., Jaffe, D. T., & Zhu, Q. 2002, PASP, 114, 153
Lefèvre, F., & Forget, F. 2009, Nature, 460, 720
Millour, E., Forget, F., Spiga, A., et al. 2015, in European Planetary Science Congress 2015 (EPSC2015), 27 September–2 October 2015, Nantes, France, EPSC2015-438, 10
Mumma, M. J., Novak, R. E., DiSanti, M. A., & Bonev, B. P. 2003, in Bull. Am. Astron. Soc., 35, 937
Mumma, M. J., Villanueva, G. L., Novak, R. E., et al. 2009, Science, 323, 1041
Richter, M. J., Ennico, K. A., McKelvey, M. E., & Seifahrt, A. 2010, in Proc. SPIE, 7735, 77356Q
Roos-Serote, M., Atreya, S. K., Webster, C. R., & Mahaffy, P. R. 2016, J. Geophys. Res. (Planets), 121, 2108
Rothman, L., Jacquemart, D., Barbe, A., et al. 2005, J. Quant. Spectrosc. Radiat. Transf., 96, 139
Rothman, L. S., Gordon, I. E., Babikov, Y., et al. 2013, J. Quant. Spec. Radiat. Transf., 130, 4
Ruyten, W. 2004, J. Quant. Spec. Radiat. Transf., 86, 231
Villanueva, G. L., Mumma, M. J., Novak, R. E., et al. 2013, Icarus, 223, 11
Warren, S. G. 1984, Appl. Opt., 23, 1206
Webster, C. R., Mahaffy, P. R., Atreya, S. K., et al. 2013, Science, 342, 355
Webster, C. R., Mahaffy, P. R., Atreya, S. K., et al. 2015, Science, 347, 415
Wiscombe, W. J. 1980, Appl. Opt., 19, 1505
Wolff, M. J., & Clancy, R. T. 2003, J. Geophys. Res. (Planets), 108, 1
Young, E. T., Becklin, E. E., Marcum, P. M., et al. 2012, ApJ, 749, L17